Fibrillation properties of human α1-acid glycoprotein

ARTICLE *in* BIOCHIMIE · SEPTEMBER 2012

Impact Factor: 2.96 · DOI: 10.1016/j.biochi.2012.09.005 · Source: PubMed

4 AUTHORS:

Andrea Scirè
Università Politecnica delle Marche
54 PUBLICATIONS **509** CITATIONS
SEE PROFILE

Maurizio Baldassarre
Stockholm University
16 PUBLICATIONS **33** CITATIONS
SEE PROFILE

Roberta Galeazzi
Università Politecnica delle Marche
51 PUBLICATIONS **404** CITATIONS
SEE PROFILE

Fabio Tanfani
Università Politecnica delle Marche
129 PUBLICATIONS **2,304** CITATIONS
SEE PROFILE

Biochimie 95 (2013) 158–166

Contents lists available at SciVerse ScienceDirect

Biochimie

journal homepage: www.elsevier.com/locate/biochi

Research paper

Fibrillation properties of human α_1-acid glycoprotein

Andrea Scirè [1], Maurizio Baldassarre [1], Roberta Galeazzi, Fabio Tanfani*

Dipartimento di Scienze della Vita e dell'Ambiente, Università Politecnica delle Marche, Via Ranieri, 60131 Ancona, Italy

ARTICLE INFO

Article history:
Received 2 July 2012
Accepted 7 September 2012
Available online 17 September 2012

Keywords:
α_1-Acid glycoprotein
Orosomucoid
Protein aggregation
Amyloid-like fibrils
Nanostructures

ABSTRACT

Human α_1-acid glycoprotein (AGP) is a positive acute phase plasma protein containing two disulfide bridges. Structural studies have shown that under specific conditions AGP undergoes aggregation. In this study, we analysed the nature of AGP's aggregates formed under reducing and non-reducing conditions at pH 5.5 and at relatively low temperatures. Thioflavin T and Congo red spectroscopic analyses indicated the presence of cross-β structures in both unreduced and reduced AGP aggregates. In these samples amyloid-like fibrils were detected by transmission electron microscopy. The fibrils are branched and bent and present in very large amount in reduced AGP. Kinetics of AGP fibrillation proceeds without a lag phase and the rate constants of cross-β formation are linearly dependent on AGP concentration and result higher under reducing conditions. The data suggest a possible downhill mechanism of polymerization with a first-order monomer concentration dependence. Bioinformatics tools highlighted an extended region that sheathes one side of the molecule containing aggregation-prone regions. Reducing conditions make the extended region less constricted, allowing greater exposure of aggregation-prone regions, thus explaining the higher propensity of AGP to aggregate and fibrillate.

1. Introduction

Human α_1-acid glycoprotein (AGP), also known as orosomucoid, belongs to the lipocalin superfamily. It is a positive acute phase protein present in plasma at high concentration (~70 mg/100 mL). The protein has two disulfide bridges and five glycan chains that contribute approximately to 45% of the total AGP's mass (41–43 kDa) [1,2]. The glycosylation pattern can change in response to systemic tissue injury, inflammation or infection, but also as a consequence of pathological conditions, such as rheumatoid arthritis, liver cirrhosis and hepatitis [1]. The theoretical pI calculated from the unglycosylated polypeptide is 4.98, whilst the low measured isoelectric point (pI) of 2.8–3.8 is due to the contribution of sialic acid present in the glycan chains (~12%).

As a member of the lipocalin superfamily, the glycoprotein has the ability to bind and transport several basic and neutral drugs and other molecules of endogenous and exogenous origin [1]. A number of other activities *in vitro* and *in vivo* has been described [3–6] but the definitive biological role of AGP has not yet been elucidated.

Recently, a detailed analysis of AGP's structure under non-reducing conditions at different pHs, revealed that within specific temperature ranges, a molten globule-like state forms [7,8]. Furthermore, AGP aggregates at acidic pHs, both under reducing and non-reducing conditions [8]. The aggregation process, however, proceeds differently and to various extents depending on specific conditions of pH, temperature and reducing environment, suggesting the possible formation of different types of aggregates.

Aggregation is quite a common feature of proteins that undergo denaturation. In most cases, the aggregates are amorphous whilst sometimes, and under specific conditions, amyloid-like fibrils may form. These are polypeptide aggregates with a core formed by a cross-β structure, i.e by β-strands extended transversely to the main fibril axis [9]. Such structures play a key role in different pathogeneses of neurodegenerative diseases such as Parkinson, Huntington, Alzheimer, and Creutzfeldt-Jakob [9]. At present, more than 20 proteins and peptides are known to be associated with amyloid diseases [9]. Amyloid fibrils themselves seem to be relatively innocuous whereas prefibrillar aggregates appear to exert cytotoxicity for their ability to permeabilize biomembranes [10] or because of the exposure of hydrophobic residues, normally buried in the folded proteins, that may promote unwanted reactions [11]. In addition to proteins forming amyloid fibrils *in vivo*, a number of non-disease associated proteins and peptides have been found to be able to form cross-β structures *in vitro* including serum albumin [12–14]. These observations have led to the concept that amyloid formation is a general property of polypeptide chains [15]. For their

Abbreviations: AGP, α_1-acid glycoprotein; u-AGP, unreduced AGP; r-AGP, reduced AGP; FT-IR, Fourier transform infrared; Amide I′, amide I band in D_2O medium; TCEP, tris(2-Carboxyethyl) phosphine; ThT, thioflavin T; CR, Congo red; TEM, transmission electron microscopy.

* Corresponding author. Tel.: +39 071 2204687; fax: +39 071 2204398.
E-mail address: f.tanfani@univpm.it (F. Tanfani).

[1] These authors contributed equally to the work.

0300-9084/$ – see front matter © 2012 Elsevier Masson SAS. All rights reserved.
http://dx.doi.org/10.1016/j.biochi.2012.09.005

implication in various medical disorders, amyloid formation is of great interest in Medicine. However, the particular physical properties of amyloid fibrils such as stability, mechanical strength, and resistance to degradation, make these structures interesting also for other disciplines, such as chemistry, physics, material and food science [16,17].

To gain more insights on AGP's aggregation process, we analysed in detail AGP aggregates formed at mild pH, i.e. at pH 5.5 (close to the pI) and at relatively low temperatures, by using different approaches such as FT-IR spectroscopy, transmission electron microscopy (TEM), Congo red (CR) and thioflavin T (ThT) spectroscopy assays. The analyses indicated that during the aggregation process, cross-β structures form. This result was confirmed by detection of amyloid-like fibrils by TEM. The fibrillation of AGP proceeded without a lag phase and was faster under reducing conditions. Bioinformatics tools identified the most aggregation-prone regions of AGP and allowed to explain the faster fibrillation of reduced AGP.

2. Material and methods

2.1. Materials

α_1-Acid glycoprotein from human plasma (AGP), piperazine, thioflavin T (ThT), Congo red (CR), lead citrate, deuterium oxide (99.9% D_2O), DCl, NaOD, Tris(2-Carboxyethyl) phosphine (TCEP) were purchased from Sigma–Aldrich. All other chemicals used were commercial samples of the purest quality. Carbon-coated 300-mesh copper grids were obtained from Ted Pella, Inc. (Redding, CA).

2.2. Detection of aggregates and amyloid fibrils

FT-IR spectroscopy was used to detect protein aggregation in AGP samples under different conditions. The presence of amyloid-like fibrils was established by the positive results of typical tests such as (a) Congo red (CR) spectroscopic assay, (b) thioflavin T (ThT) spectroscopy assay, (c) transmission electron microscopy (TEM) [18].

2.3. Preparation of samples for infrared spectroscopy measurements

For each sample, 1.5 mg AGP was dissolved in 200 μl of 50 mM piperazine/DCl buffer pD 5.5 (buffer A), or in 200 μl of 50 mM piperazine/DCl, 5 mM TCEP buffer pD 5.5 (buffer B). Each protein sample was centrifuged in a "30K Amicon ultra 0.5" micro concentrator (Millipore Ireland Ltd, Cork, IRL) at 3000× *g*, 4 °C, until the volume solution reached approximately 40 μl. Then, further 200 μl of chosen buffer (A, B) were added and the solution was re-concentrated. This procedure was repeated five times in order to completely hydrate AGP with the chosen buffer. The final concentration of the protein solution for analysis was approximately 30 mg/mL. The pD value was measured with a standard pH electrode, and the value was corrected according to pD = pH + 0.4 [19].

2.4. Infrared spectra

The concentrated protein sample was injected into a thermostatted Graseby Specac 20500 cell (Graseby-Specac Ltd, Orpington, Kent, UK) fitted with CaF_2 windows and a 25 μm mylar spacer. FT-IR spectra were recorded on a Perkin–Elmer 1760-x Fourier transform infrared spectrometer using a deuterated triglycine sulphate detector and a normal Beer-Norton apodization function. At least 24 h before, and during data acquisition, the spectrometer was continuously purged with dry air at a dew point of −70 °C. To obtain spectra at different temperatures, an external bath circulator (HAAKE F3) was used. Spectra were collected every 5 °C, in the 20–90 °C temperature range. The actual temperature in the cell was controlled by a thermocouple placed directly onto the windows. Spectra of buffers and samples were acquired at 2 cm^{-1} resolution under the same scanning and temperature conditions. Correct subtraction of D_2O was adjusted to the removal of the D_2O bending absorption close to 1220 cm^{-1} [20]. Spectra were processed using the SPECTRUM software from Perkin–Elmer. The deconvoluted parameters were set with a gamma value of 2.5 and a smoothing length of 60.

2.5. Preparation of samples for CR, ThT and TEM analyses

Samples of AGP at various concentrations (1, 2 and 5 mg/mL) were prepared by directly dissolving the lyophilized protein in 50 mM piperazine/HCl buffers at pH 5.5, in the absence or presence of the 5 mM reducing agent TCEP. An additional AGP sample at 0.3 mg/mL was prepared for the analysis under reducing conditions. The samples were incubated on a thermostated tube plate (Thermo Twister Comfort, Quantifoil Instruments GmbH, Jena, Germany) kept at an orbital shaking speed of 500 rpm. The incubation temperature corresponded to the one at which the aggregation onset was observed in infrared measurements of AGP under each of the two buffer conditions described above. More specifically, the protein samples in the absence and in the presence of the reducing agent TCEP, were incubated at 60 °C and 45 °C, respectively. Aliquots of appropriate volumes were withdrawn from each sample prior to incubation at the desired temperature in order to be used as control samples in subsequent analyses. The typical overall incubation time was 6 h, which was occasionally extended up to 30 or 48 h for selected samples.

2.6. Congo red (CR) spectroscopic assay

Aliquots of AGP samples (5 mg/mL) were collected at the end of 6 h incubation under specific temperature and buffer conditions. The binding of CR to AGP was evaluated by measuring the absorbance of the dye in the absence and in the presence of the protein samples in the 400–700 nm range. For these experiments a Shimadzu UV-2401PC spectrophotometer was used. All measurements were made by firstly collecting the spectrum of 25 μM CR in 5 mM potassium phosphate, 150 mM NaCl, pH 7.4 (control). Under these conditions, the absorbance spectrum of CR displayed a maximum at 490 nm. AGP samples were then added to the CR solution to a final CR/AGP molar ratio of 8, which is suggested to be the optimal test condition [21]. After 40 min of CR/AGP incubation, the spectrum was collected. A red shift in the CR/AGP spectrum with respect to the CR spectrum is indicative of the presence of cross-β structures [18].

2.7. Thioflavin T spectroscopic assay

Aliquots from the samples under incubation were withdrawn at definite time points. The denaturation/aggregation processes were stopped by incubation on ice. The aliquots were then diluted in a 1-cm quartz cuvette to 1.2 mL with freshly prepared 10 mM phosphate buffer, pH 7.0, containing 150 mM NaCl and Thioflavin T at an appropriate concentration. The final concentrations of ThT and AGP in the assay mixture was 25 and 1.7 μM, respectively, which yields an optimal molar ratio of 15 (μM probe/μM protein), as reported elsewhere [21].

The fluorescence emission of protein-bound ThT was measured on a Perkin–Elmer LS55 spectrofluorimeter by irradiating the

samples with incident light at 440 nm and integrating the emission intensity at 482 nm over 60 s. The excitation and emission slits were set to 5 and 10 nm, respectively. All values were corrected by subtracting the emission intensity of the control samples. The corrected emission intensities were plotted versus the corresponding incubation time and fitted to a first order exponential decay function using OriginPro 7.5 software (OriginLab, Northampton, MA).

2.8. Transmission electron microscopy (TEM)

The 6 h-treated AGP solutions were diluted to 0.5 or 1 mg/mL and then a 2 μL drop of the diluted solution was placed onto carbon-coated 300-mesh copper grids. Occasionally, the samples incubated for 30 or 48 h were also examined. The samples were left to adsorb for 10 min. The excess of solution was removed by blotting it with a small piece of filter paper placed on the border of the grids. The samples were stained with a 2 μL drop of 0.25% (w/v) lead citrate solution for 3 min. The excess stain was removed by a tiny piece of filter paper and the grids gently washed three times with a 2 μL drop of distilled water and then left to dry off [22]. The samples were examined on a Philips 208 transmission electron microscope at an accelerating voltage of 80 kV.

2.9. Assessment of solvent accessibility and prediction of aggregation-prone regions

The degree of exposure of single protein residues to solvent was assessed by submitting the crystallographic structure of AGP (PDB ID: 3KQ0) to the ASAView server (http://gibk26.bio.kyutech.ac.jp/jouhou/shandar/netasa/asaview/) [23]. Water molecules as well as any other non-protein compound were removed from the coordinate file prior to submission. The size of the water probe was left as default (1.4 Å). Residues showing values above 50% or below 20% are considered to be exposed or buried, respectively. Residues with values between 20% and 50% are considered to be only partially exposed.

The prediction of aggregation-prone regions was performed by submitting the amino acid sequence of mature AGP to the AGGRESCAN server (http://bioinf.uab.es/aggrescan/) [24].

2.10. Preparation of protein structures for MD simulations

The crystallographic structure of AGP was retrieved from the Brookhaven Protein Databank (PDB ID: 3KQ0). Missing hydrogens were added using the CHIMERA software [25]. The protonation state of ionizable groups was adjusted according to the desired pH of the simulation (7.4 and 5.5). Other parameters were set as follows: salinity 0.15, internal dielectric 6, external dielectric 80 [26]. For simulation under reducing conditions, the disulfide bridges in the structure prepared at pH 5.5 were converted into the corresponding thiols. The simulation temperature was 60 °C for the structures containing oxidized disulfide bridges at both pH 7.4 and 5.5, and 45 °C for the structure containing reduced disulfides at pH 5.5.

2.11. MD simulation protocol

Computation of each MD trajectory was performed in parallel at a speed of 4 ns/day on an SP6 IBM workstation. Before the MD simulations, the starting geometries were minimized with the AMBER11 software package [27] using the AMBER force field [28] and the TIP3P water model. Periodic boundary conditions were applied to the protein system. Each structure was initially minimized with a derivative convergence criterion of 0.05 kJ $Å^{-2}$ mol (2500 steps with steepest descent followed by 2500 steps with conjugate gradient). Each structure was then heated to the final temperature of simulation in 40 ps (1-fs time step), and let to equilibrate for another 40 ps before starting data collection. The SHAKE algorithm was used to constrain the stretching of hydrogen-involving bonds [29]. Equilibrated structures were used as starting points for 20-ns production trajectories, performed at constant pressure (1 atm) and temperature (NPT ensemble) using standard coupling schemes (the same in all cases). Results reported in the literature [30] strongly suggest that 10 ns is long enough for simulations for many analysis purposes and confirm that the current computational protocol is able to recognize strong denaturing conditions that start protein unfolding (which might take micro- to milliseconds to complete) in the 0- to 30-ns simulation window. Particle Mesh Ewald approaches were used to deal with long-range effects [31]. The system coordinates were saved to trajectory files every 10 ps. Trajectories were analysed to obtain structural and dynamic properties. Structural descriptors include backbone RMSD, solvent accessible surface for all heavy atoms, secondary structure, solvent contact profiles, and others. The analysis of the MD trajectories was performed within the Sirius 1.2 [32] and CHIMERA software [25].

3. Results and discussion

3.1. Acidic environment, high temperatures and disulfide bonds reduction decrease protein stability and promote aggregation

Sulfhydryl reductants are widely used in protein chemistry and biochemistry to investigate on the role of disulfide bridges on protein stability and function. The most commonly used disulfide reductants are thiols like 2-mercaptoethanol and dithiothreitol (DTT). In many cases, studies on protein fibrillation *in vitro* require a long incubation (even days) of the sample at acidic pHs and high temperatures. Under these conditions, the above chemicals might not be stable and hence the experiment would give incorrect results [33]. In our experiments we used tris(2-Carboxyethyl) phosphine (TCEP) as a sulfhydryl reductant since it has been demonstrated to be very stable under the conditions above described [33].

Fig. 1 (A and B) reports the temperature-dependent changes in the deconvoluted infrared spectra of AGP samples at pD 5.5 in the absence and in the presence of TCEP, respectively. The spectra at 20 °C display three main bands ascribed to the secondary structural elements present in the typical lipocalin fold of AGP, which comprise an eight-stranded β-barrel flanked by an α-helix [2]. The bands are located close to 1634 (β-sheet), 1691 (β-sheet) and 1651 cm^{-1} (α-helix) [8]. With the increase in temperature, the intensity of the α-helix and β-sheet bands decreases, indicating protein denaturation. Furthermore, the increase in temperature also causes the formation of two new bands close to 1615 and 1684 cm^{-1} (marked with the symbol *). These two bands are characteristic of intermolecular interactions (aggregation) brought about by protein denaturation [34]. Thus, the data indicate that at pD 5.5 the increase in temperature causes concomitant denaturation and aggregation of AGP molecules. Under non-reducing conditions, the onset temperature of aggregation (marked with the symbol §) is at 60 °C. Under reducing conditions, the onset temperature of aggregation is at 45 °C and the aggregation propensity of AGP is greater with respect to the protein in the absence of TCEP (compare aggregation band intensities). Noteworthy is the absence of aggregation at pH 7.4 [7,8].

Temperature-induced protein aggregation usually leads to amorphous aggregates with a milky appearance. Sometimes, and under specific conditions, the aggregated protein has a gel-like

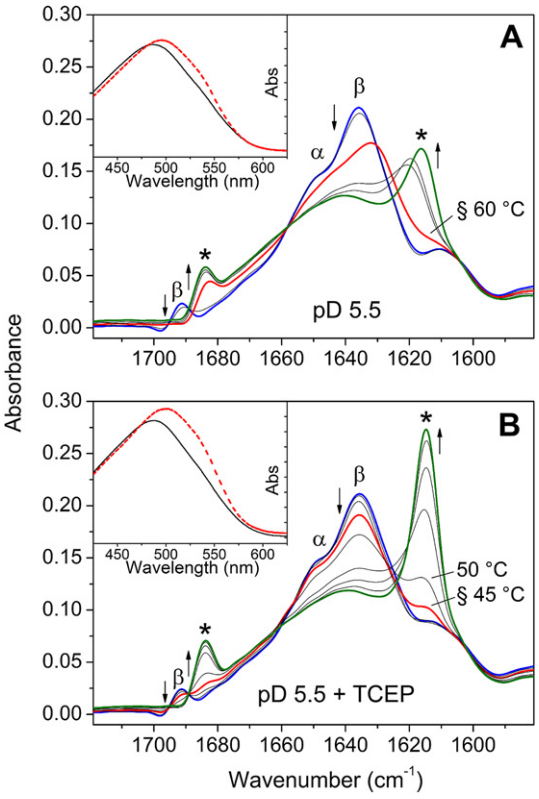

Fig. 1. Infrared and CR spectroscopic analyses, Panels (A and B): experiments performed under non-reducing and reducing conditions, respectively. The two panels display the deconvoluted IR spectra of AGP at pD 5.5. In each panel, eight spectra in the 20–90 °C temperature range with 10 °C increments are shown. In panel (B) an additional spectrum obtained at 45 °C is also shown. The symbol (β) indicates the β-sheet bands close to 1634 and 1691 cm^{-1}. The symbol (α) highlights the α-helix band. The aggregation bands are marked with the symbol (*). The spectrum revealing the onset of aggregation is marked with the symbol (§) and is displayed in red. The arrows (↑) and (↓) indicate the temperature-dependent increase and decrease of the corresponding band intensities, respectively. The blue and green spectra were obtained at 20 °C and 90 °C, respectively. Insets in panels (A, B): absorption spectra of CR in the absence (continuous black lines) and in the presence (dashed red lines) of AGP samples heated for 6 h at temperatures corresponding to the onset of aggregation i.e. at 60 and 45 C° for unreduced and reduced AGP, respectively. (For interpretation of the references to colour in this figure legend, the reader is referred to the web version of this article.)

appearance which might be indicative of amyloid-like fibril formation [18]. Both amorphous and amyloid-like fibril display aggregation bands but the infrared spectrum is not able to distinguish the kind of aggregation. However, in our case all AGP heated samples had a gel-like appearance suggesting the possible presence of amyloid-like fibrils.

3.2. Unreduced and reduced AGP aggregate into amyloid-like structures

Preliminary experiments on binding of ThT and CR to AGP samples were undertaken to find the best conditions for cross-β structures [9] formation and detection. We decided to analyse the aggregation process at the onset temperature of protein aggregation/denaturation in order to slow down the aggregation process that is very rapid at high temperatures (data not shown). Moreover, the choice of the onset temperature of protein aggregation/denaturation allows to normalise the process of aggregation against the extent of AGP unfolding under different conditions (reduced and unreduced AGP).

Insets in Fig. 1, panels (A, B) show the absorption spectra of CR in the absence (continuous lines) and in the presence (dotted lines) of AGP samples heated for 6 h at temperatures corresponding to the onset of protein aggregation i.e. at 60 and 45 °C for unreduced and reduced AGP, respectively. A red-shift in the CR spectrum was observed in both cases, indicating the presence of cross-β structures in the samples [18].

3.3. AGP fibrillation follows a single exponential trend over time, with no apparent lag phase

The fluorescent dye Thioflavin T (ThT) is the most widely used probe for the identification of amyloid fibrils *in vitro*, in biopsies, or in *ex vivo* post mortem samples [35,36]. The remarkable enhancement of its fluorescence emission upon binding to fibrils makes ThT a particularly powerful and convenient tool to study fibrillation kinetics. Protein aggregation reactions leading to protofibril and fibril formation are often evaluated in terms of nucleation-dependent polymerization (NDP) model [37]. The NPD model resembles crystallization processes in which nucleation is the rate-determining step followed by a rapid growth phase. The formation of a nucleus implies the presence of a lag phase in which the lag time increases with the decrease in protein concentration and decreases upon seeding.

The fluorescence emission of ThT shows an increase over time in all AGP samples incubated under aggregation-inducing conditions, with no apparent lag phase in unreduced (u-AGP) and reduced AGP (r-AGP) (Fig. 2 A and B, respectively), indicating that the fibrillation process does not follow a canonical nucleation-dependent polymerization [18,37]. The fluorescence emission seems to be linearly dependent on u-AGP concentration (Fig. 2A), whilst in the case of r-AGP at 5, 2 and 1 mg/mL concentration, fluorescence hardly seems to be dependent on protein concentration, having reached the value of about 200 after 6 h (Fig. 2B). On the other hand, the fluorescence intensity is approximately halved for r-AGP concentrations of 0.3 mg/mL. More detailed information was obtained by fitting the data reported in Fig. 2A and B with a first order exponential function for determining the rate constants (k) of cross-β formation (Fig. 2C). At pH 5.5 under non-reducing conditions, the rate constants increase linearly with the increase in u-AGP concentration. Under reducing conditions the (k) values are higher than those related to u-AGP at the corresponding concentrations, and they are also linearly dependent on protein concentration (Fig. 2C). However, the rate constants are less affected by protein concentration than in the case of u-AGP.

The ThT experimental data of u-AGP and r-AGP indicate that the latter has a higher propensity to undergo aggregation. Indeed, this is also indicated by the infrared spectra which show a higher intensity of aggregation bands in r-AGP compared to u-AGP (Fig. 1). The high propensity of r-AGP to form cross-β structures might be due to aggregation-prone regions that are partially or totally buried in u-AGP and become available upon AGP reduction as a consequence of conformational changes. The high aggregation propensity of r-AGP could also be due to the higher molecular flexibility that would facilitate favourable intermolecular interactions leading to aggregation.

The absence of a lag phase has been observed in some amyloidogenic proteins such as transthyretin [38], barstar [37], bovine and human serum albumin [12–14], among others. Some kinetic models may explain and fit with data lacking a lag phase but, given the complex nature of aggregation kinetics [39], it is difficult to assign unequivocally a particular kinetic pathway to AGP. However, studies on transthyretin [38] and on bovine [13] and human [14] serum albumin seem to share similar features with AGP fibrillation. In these studies, the authors suggested a downhill

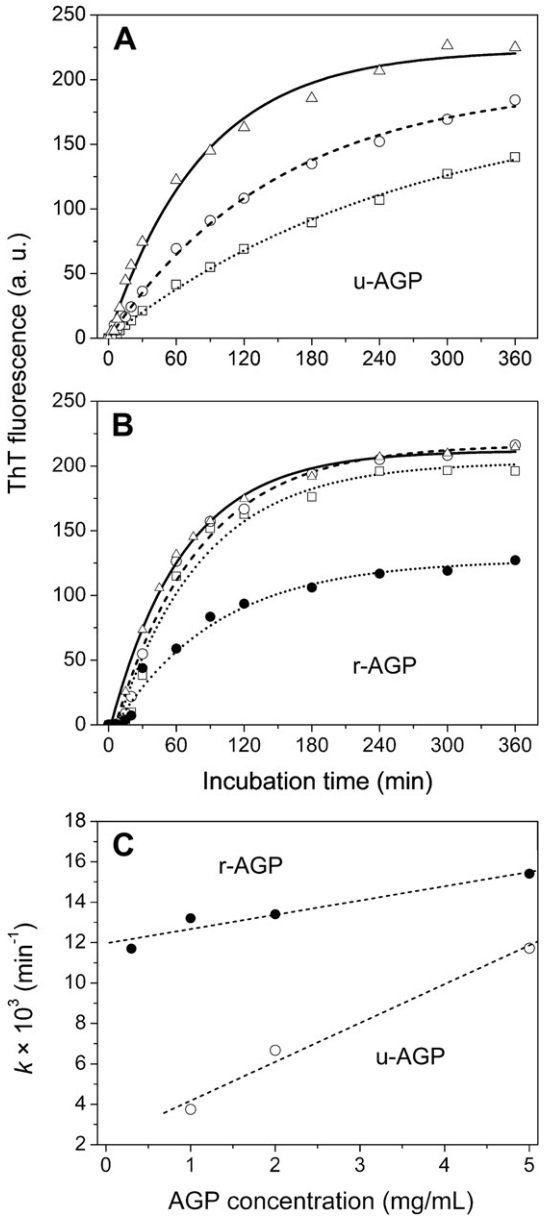

Fig. 2. Kinetics of cross-β formation obtained by the ThT spectroscopic assay, Panels (A and B): AGP samples at pH 5.5 under non-reducing and reducing conditions, respectively. The symbols (●) (□), (○), and (△) refer to AGP samples at 0.3, 1, 2 and 5 mg/mL, respectively. Samples were incubated at temperatures corresponding to the onset of aggregation, i.e. at 60 and 45 C° for unreduced and reduced AGP, respectively. Panel (C): Plot of the rate constants (k) as a function of protein concentration. u-AGP and r-AGP stand for unreduced and reduced AGP, respectively. The R^2 values vary within 0.9937–0.9983 and within 0.9807–0.9943 for u-AGP and r-AGP, respectively.

polymerization that does not invoke a thermodynamic nucleus, which is the central feature of the NDP model. Instead, the model considers the transformation of a native protein into an amyloidogenic monomer that assembles into soluble aggregates which lead to fibrillation. In our case, the amyloidogenic monomer of r-AGP would have a higher ability to undergo favourable molecular interaction and the soluble aggregates would form more rapidly than u-AGP.

According to the model, in a downhill polymerization, each step is essentially irreversible (with a first-order monomer concentration dependence) and the highest energy species under partially denaturing conditions is the native monomer [38].

3.4. Reduction of disulfide bridges increases fibril length and induces branching

TEM analysis of AGP samples after treatment at specific temperatures and pH values shows different protein aggregates of different size and form. Most of them appear as AGP amorphous assemblies or large aggregates with needle-like protrusions (not shown) that have been observed also for transthyretin [40]. These data suggest that the large particles observed may contain regular structures. Detailed inspection of the carbon-coated copper grids, besides large aggregates, also reveals the presence of typical amyloid-like fibrils (Fig. 3). Unreduced AGP at pH 5.5 and 60 °C produced short fibrils similar to rod-like structures 8–12 nm till 20–30 nm thick. Longer fibrils were also detected (not shown). Besides these, a fibril with a rope-like structure was detected (Fig. 3B). It appears as two twisted protofilaments, each approximately 20 nm thick. The twist is left-handed with a pitch of about 35–40 nm. Similar structure have also been found in other protein aggregates [41,42].

AGP at pH 5.5 and at 45 °C under reducing conditions, produced a large number of fibrils shown in Fig. 3C–F at different magnifications. A large amount of fibrils were observed after 48 h of incubation. In this sample the presence of amorphous assemblies and big aggregates was negligible. Most of the squares composing the carbon-coated copper grids were full of long and branched fibrils (Fig. 3C). These have a thickness varying between 10 and 20 nm, with a branching angle of about 60° (or 120° depending how the fibril is observed) (Fig. 3D–F). In some instances, the fibrils were bent with a bending angle of about 120° (e.g. arrows in Fig. 3G,F). Fig. 3F highlights the connections between the fibrils and the 120° bending angle present in one fibril.

3.5. Aggregation-prone regions can be detected in the sequence of AGP

In an attempt to explain the higher rate constant (k) of cross-β formation under reducing conditions (Fig. 2C), we used ASAView and AGGRESCAN softwares to assess the degree of exposure of single protein residues to the solvent and to predict the aggregation-prone regions, respectively (Fig. 4A). AGGRESCAN analysis predicted the presence of eight potentially aggregation-prone regions in the primary structure of mature AGP. These regions are numbered 1–8 consistently with their position along the amino acid sequence. Regions 1, 2 and 3 show the highest aggregation scores (0.43–0.45), while regions 4, 5 and 6 show intermediate scores (0.25–0.31). Regions 7 and 8 show the lowest score (0.14). The regions mentioned above are highlighted in different colours (red: highest scores; orange: intermediate scores; yellow: lowest scores) in Fig. 4A and in the cartoon representation of human AGP (Fig. 4B and C). A visual inspection of Fig. 4B reveals that regions 2 to 7 are partially or totally embedded in the β-barrel. Region 1 lies in the short *N*-terminal α-helix, whilst region 8 lies in part in the longer α-helix involved in the Cys5-Cys147 disulfide bridge.

Rotation of the AGP structure (4B) by 180° yields cartoon (4C). This figure shows in more detail that the α-helix at the C-terminal is connected to the α-helix close to the N-terminal *via* a long loop containing two short helices (blue part of the cartoon). This extended region almost entirely sheathes one side of the barrel and is anchored to the bulk structure *via* disulfides Cys5–Cys147 and Cys72–Cys165. It is noteworthy that five of the potentially aggregation-prone regions (2, 3, 5, 6 and 7) are partially or totally covered by the long blue region of the cartoon that seems to protect these regions from solvent exposure. Indeed, a particularly low

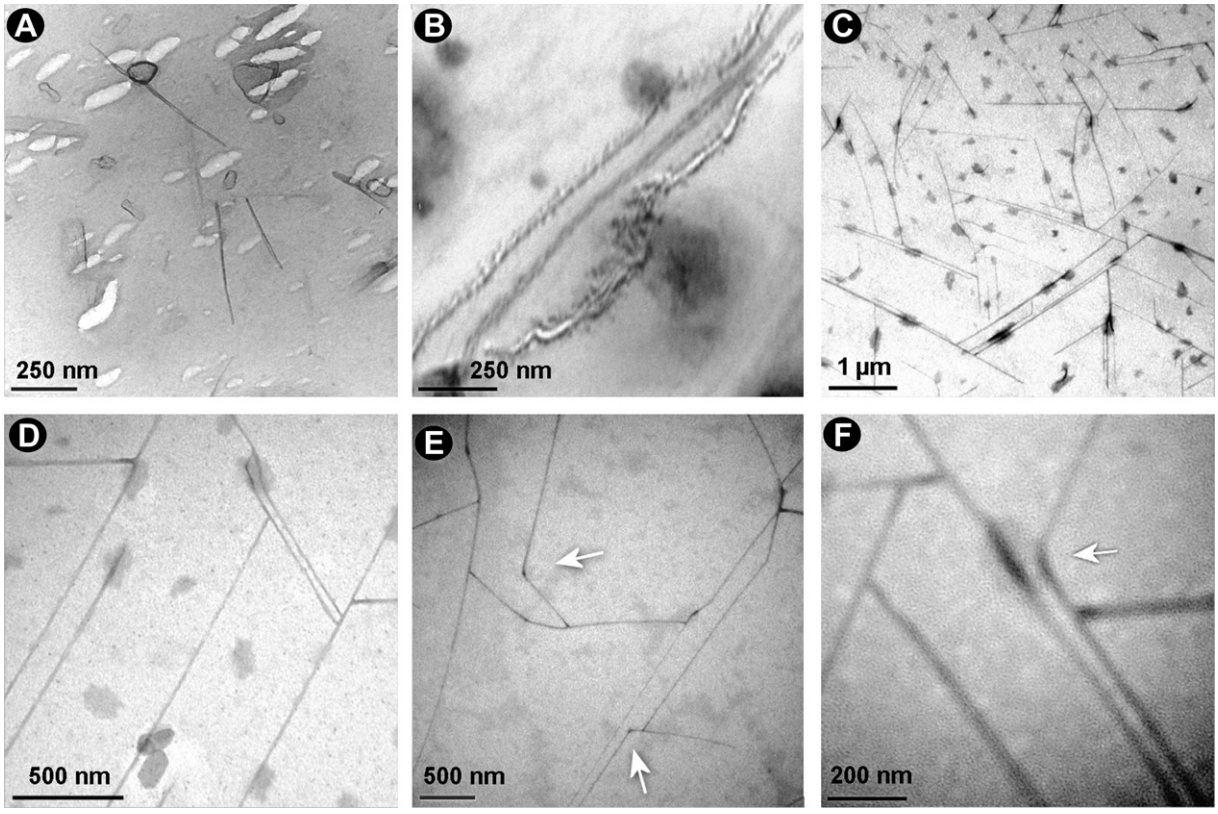

Fig. 3. TEM analysis Bars in panels (A–F): 250 nm, 250 nm, 1 µm, 500 nm, 500 nm, and 200 nm, respectively. Panels (A, B): unreduced AGP at pH 5.5 heated at 60 °C. Panels (C–F): reduced AGP at pH 5.5 heated at 45 °C. Large amounts of fibrils were observed after 48 h incubation. In panels (C–F) the fibrils show branches with branching angles of about 60°. The arrows in panels (E and F) indicate a 120° bending angle in some fibrils.

accessibility of the solvent to regions (2, 3, 5, 6 and 7) is shown by the ASAView results (see grey bars in Fig. 3A).

The observation that the long blue region of the protein is anchored to the main scaffold via two disulfide bridges, and that seems to hide several aggregation-prone regions from the solvent, might explain the increased instability and aggregation propensity of AGP observed under reducing conditions in both FT-IR measurements and Thioflavin T-binding kinetics. Indeed, after

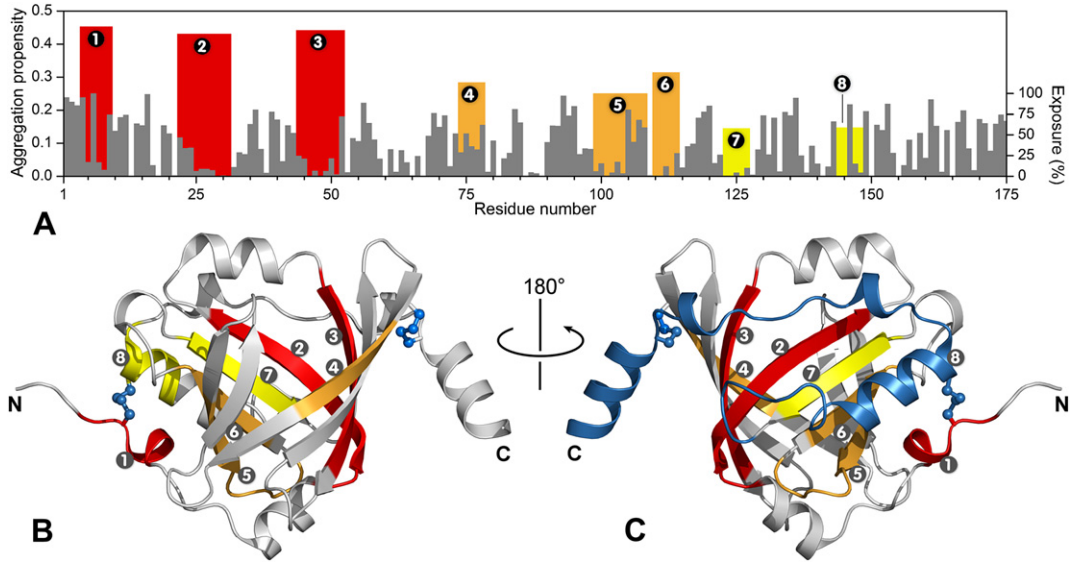

Fig. 4. Degree of exposure to solvent of AGP residues and prediction of aggregation-prone regions, Upper graph (A): grey bars represent the degree of exposure (%) to solvent of AGP residues. Aggregation-prone regions are represented by (1–8) bars. Red bars (1–3), orange bars (4–6) and yellow bars (7, 8) represent high, medium and low aggregation propensity, respectively. Cartoon (B): crystal structure of recombinant human AGP at 1.8 Å resolution (PDB ID:3KQ0). Disulfide bridges are shown in ball-and-stick mode. Numbers (1–8) represent the aggregation-prone regions, shown with different colours, corresponding to the bars (1–8) in the upper panel. Cartoon (C): crystal structure of recombinant human AGP rotated by 180° with respect to cartoon (B). The blue colour highlights the AGP region that becomes less constricted after disulfide reduction. (For interpretation of the references to colour in this figure legend, the reader is referred to the web version of this article.)

disulfide reduction it is reasonably expected that this AGP region may become less constricted, allowing a higher exposure of the (2, 3, 5, 6 and 7) regions.

Molecular Dynamics simulations were performed to assess whether the combination of pH, temperature and disulfide redox state used in our FT-IR and ThT-binding measurements might lead to exposure of aggregation-prone regions and, thus, explain the aggregation properties observed experimentally.

3.6. Molecular dynamics reveal a higher flexibility and an enhanced exposure of aggregation-prone regions in r-AGP

The native fold of AGP is strictly conserved throughout the MD simulation at pH 7.4, 60 °C (20 ns), as well as during the preceding heating and equilibration steps (40 + 40 ps). In addition, the solvent exposure of the most populated clusters detected during the simulation does not show significant increase with respect to that of the starting structure (data now shown).

In a similar way, the fold and secondary structure content of AGP do not change during the heating and equilibration steps performed at pH 5.5, 60 °C. The RMSD calculated for the Cα at the end of this phase is as low as 0.6 Å, indicating that the overall conformation of the polypeptide chain strictly resembles the starting structure. At $t = 2.7$ ns and upwards, however, an evident motion of the α-helices in the vicinity of the disulfide bridges can be observed. In particular, a partial unfolding/refolding of the C-terminal α-helix (Lys161–Glu175) occurs simultaneously with the stretching of the Cys72-Cys165 S–S bond. Superimposition of the four most populated clusters with the starting structure (Fig. 5, panel A) allows for a visual inspection of the most evident conformational fluctuations occurring during the MD trajectory. The fraying of the C-terminal α-helix described above exposes, at least partially, two of the regions detected with AGGRESCAN (regions 3 and 5) (Figs. 4 and 5C). Solvent exposure analysis of the clusters with ASAView confirmed this observation (Fig. 5, panel C, upper row). In addition, a partial unfolding can be detected in proximity of the disulfide bridge near the N-terminus (Cys5–Cys147). An increased flexibility of the Ile2-Ala16 region is evident, leading to loss of the short α-helix segment contained therein and greatly enhancing solvent exposure of AGGRESCAN-detected region 1 (Fig. 5, panel C, upper row). Increased flexibility is displayed also by regions Ser89–Glu96 and Leu101–Leu104. The same simulation protocol, albeit at a different temperature, was applied to investigate the structural dynamics shown by the protein following reduction of its two disulfide bridges.

It is noteworthy that the overall fold and secondary structure content is maintained during the heating and equilibration steps of AGP whose disulfide bridges had been reduced (pH 5.5, 45 °C). The RMSD at the end of this conditioning phase is only slightly greater (0.7 Å) than the one calculated under non-reducing conditions at

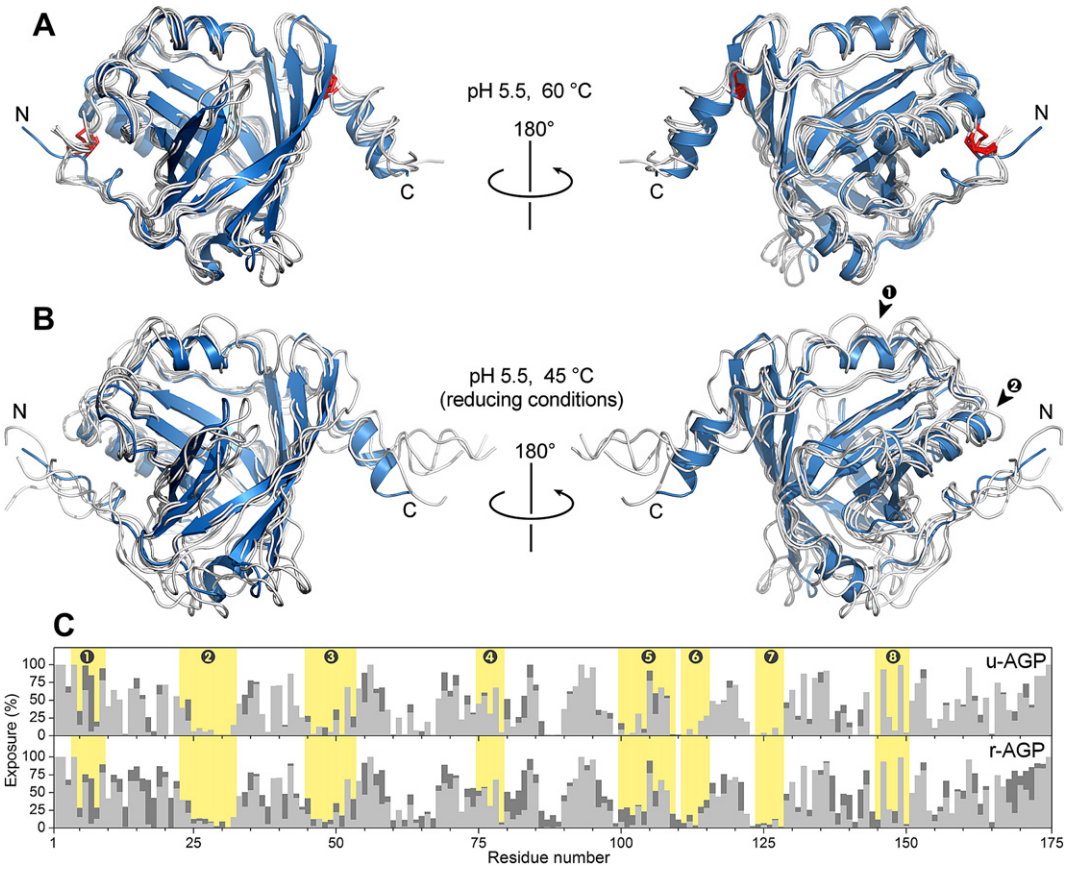

Fig. 5. Molecular dynamics of AGP at pH 5.5 under non-reducing (60 °C) and reducing (45 °C) conditions. The four most populated clusters detected during the 20-ns MD simulations of AGP under non-reducing (A) and reducing (B) conditions are shown in grey and are superimposed to the corresponding starting structure (blue cartoon). For the sake of clarity, the secondary structure features of all clusters are omitted. The disulfide bridges in panel A are shown as red sticks. Arrowheads labelled 1 and 2 in panel B denote α-helices Glu35-Val41 and Glu140-Arg149, respectively. Panel C: Averaged solvent exposure (dark grey bars) of clusters 1-4 during the MD simulations under non-reducing (top row) and reducing (bottom row) conditions. Exposure values calculated for the starting structure are shown in light grey as a reference. Yellow boxes denote the 8 aggregation-prone regions detected by AGGRESCAN. Solvent-exposure was assessed using ASAView as described in the text. (For interpretation of the references to colour in this figure legend, the reader is referred to the web version of this article.)

60 °C. However, structural fluctuations, mostly involving helical segments, occur earlier in the reduced structure than in its oxidized counterpart (Fig. 5, panel B). At $t = 2.2$ ns, massive fraying of the long C-terminal α-helix (Lys161–Glu175) and of the shorter α-helices Glu35–Val41 (Fig. 5B, arrowhead #1) and Glu140–Arg149 (Fig. 5B, arrowhead #2) takes place. Additionally, a fast, dynamic unfolding/refolding occurs around the cysteinic residues Cys72 and Cys165. Interestingly, the RMSD of the Cα atoms calculated at this time point of the trajectory (1.3 Å) is mostly due to the increased flexibility of regions Lys163–Glu175 (4.44 Å), at C-terminus, and Ile2–Ala16 (2.2 Å), at the N-terminus. As a matter of fact, at $t = 4.2$ ns, conformational fluctuations around Cys5 and Cys147 can be detected. Regions Leu101–Leu104 and Glu35–Glu43 are also involved in large RMSD variation during the simulation. The unfolding/refolding fluctuations can be detected iteratively throughout the trajectory (20 ns). The four most populated clusters detected during the simulation are depicted in Fig. 5, panel B.

As a result of the increased flexibility discussed above, several regions become more exposed to the solvent during the simulation. It is noteworthy that the AGGRESCAN-detected regions 1, 3 and 5 show increased exposure, together with part of region 2 (Fig. 5, panel C, bottom row). However, several areas of the protein structure, despite not being predicted to be aggregation-prone, display greatly increased exposure. Some of these regions lie in close proximity to the regions detected by the AGGRESCAN analysis, thus suggesting that increased flexibility and exposure of, as well as near, the potentially fibrillogenic regions, might be the cause of the enhanced aggregation of AGP observed experimentally.

The experimental and bioinformatics data show that reduction of the disulfide bridges does not merely reduces the stability of AGP, but also enhances its tendency to aggregate. Although the temperatures at which we have detected aggregation are well above the physiological ones, it must be pointed out that at slightly more acidic pH values (4.5), disulfide reduction has an even more marked effect on the onset of protein aggregation, which was measured to be as low as 35 °C [8]. Despite being well below the pH of blood, this pH value may be measured in the vicinity of cell membranes [43]. Therefore carrier and circulating proteins such as serum albumin and AGP come in contact with low-pH regions frequently [12] and therefore a reduced AGP or AGP lacking in disulfide bridges probably would undergo aggregation. This observation may lead to the speculation that nature engineered AGP with disulfide bridges to protect the molecule against potentially aggregating conditions found in our body.

4. Conclusions

In this work, the combination of different biochemical, spectroscopic and *in silico* approaches shed light on, and explained the aggregation of the highly glycosilated human α_1-acid glycoprotein (AGP) into amyloid-like fibrils under specific environmental and temperature conditions. TEM analysis of u-AGP samples shows, besides fibrils, different protein aggregates of different size and form, most of them appearing as amorphous assemblies or as large aggregates. On the other hand, r-AGP undergoes massive fibrillation producing long and branched fibrils. Kinetics of AGP fibrillation proceeds without a lag phase and the rate constants of cross-β formation are linearly dependent on AGP concentration and result higher under reducing conditions. The reduction of disulfide bonds makes the protein more flexible, allowing easier molecular interactions and formation of amyloid-like fibrils at relatively low temperature. The data suggest a possible downhill mechanism of polymerization with a first-order monomer concentration dependence. Detailed analysis of the AGP's 3D structure highlighted the presence of an extended region that sheathes one side of the molecule containing aggregation-prone regions. Molecular dynamic simulations demonstrated that upon reduction, some aggregation-prone regions become more exposed to the solvent, thus explaining the higher propensity of r-AGP to aggregate. The experimental and bioinformatics data indicate that disulfide bonds play a significant role in the AGP stabilization and reduce the AGP's propensity to aggregate at low pHs.

Acknowledgements

This work was supported by a grant from UNIVPM. We wish to thank Prof. Saverio Cinti (Dipartimento di Medicina Sperimentale e Clinica, UNIVPM, Ancona) for the access to TEM facility and Dr. Plinio Ferrara (Azienda Ospedaliero-Universitaria, Ancona) for TEM technical assistance and managing. We thank also CINECA Supercomputing Center for providing computer time on its IBM SP Power6 supercomputer (CINECA-HPC ISCRA C Grant 2011–2012) and for technical assistance.

References

[1] T. Fournier, N.N. Medjoubi, D. Porquet, Alpha-1-acid glycoprotein, Biochim. Biophys. Acta. 1482 (2000) 157–171.
[2] D.L. Schonfeld, R.B. Ravelli, U. Mueller, A. Skerra, The 1.8-A crystal structure of alpha1-acid glycoprotein (Orosomucoid) solved by UV RIP reveals the broad drug-binding activity of this human plasma lipocalin, J. Mol. Biol. 384 (2008) 393–405.
[3] D. French, J. Watson, B. McCahill, I. Taggart, K.D. Smith, A preliminary evaluation of the functional significance of alpha-1-acid glycoprotein glycosylation on wound healing, Biomed. Chromatogr. 16 (2002) 412–419.
[4] P.J. Ojala, M. Hermansson, M. Tolvanen, K. Polvinen, T. Hirvonen, U. Impola, M. Jauhiainen, P. Somerharju, J. Parkkinen, Identification of alpha-1 acid glycoprotein as a lysophospholipid binding protein: a complementary role to albumin in the scavenging of lysophosphatidylcholine, Biochemistry 45 (2006) 14021–14031.
[5] J.K. Rainey, C.K. Wen, M.C. Goh, Hierarchical assembly and the onset of banding in fibrous long spacing collagen revealed by atomic force microscopy, Matrix Biol. 21 (2002) 647–660.
[6] F. Zsila, Chaperone-like activity of the acute-phase component human serum alpha 1-acid glycoprotein: inhibition of thermal- and chemical-induced aggregation of various proteins, Bioorg. Med. Chem. Lett. 20 (2010) 1205–1209.
[7] A. Ausili, A. Scire, E. Damiani, G. Zolese, E. Bertoli, F. Tanfani, Temperature-Induced molten globule-like state in human alpha(1)-acid glycoprotein: an infrared spectroscopic study, Biochemistry 44 (2005) 15997–16006.
[8] A. Scire, M. Baldassarre, G. Lupidi, F. Tanfani, Importance of pH and disulfide bridges on the structural and binding properties of human alpha(1)-acid glycoprotein, Biochimie 93 (2011) 1529–1536.
[9] M. Stefani, C.M. Dobson, Protein aggregation and aggregate toxicity: new insights into protein folding, misfolding diseases and biological evolution, J. Mol. Med. 81 (2003) 678–699.
[10] M.J. Volles, P.T. Lansbury Jr., Zeroing in on the pathogenic form of alpha-synuclein and its mechanism of neurotoxicity in Parkinson's disease, Biochemistry 42 (2003) 7871–7878.
[11] M. Bucciantini, G. Calloni, F. Chiti, L. Formigli, D. Nosi, C.M. Dobson, M. Stefani, Prefibrillar amyloid protein aggregates share common features of cytotoxicity, J. Biol. Chem. 279 (2004) 31374–31382.
[12] M. Bhattacharya, N. Jain, S. Mukhopadhyay, Insights into the mechanism of aggregation and fibril formation from bovine serum albumin, J. Phys. Chem. B. 115 (2011) 4195–4205.
[13] N.K. Holm, S.K. Jespersen, L.V. Thomassen, T.Y. Wolff, P. Sehgal, L.A. Thomsen, G. Christiansen, C.B. Andersen, A.D. Knudsen, D.E. Otzen, Aggregation and fibrillation of bovine serum albumin, Biochim. Biophys. Acta. 1774 (2007) 1128–1138.
[14] J. Juarez, S.G. Lopez, A. Cambon, P. Taboada, V. Mosquera, Influence of electrostatic interactions on the fibrillation process of human serum albumin, J. Phys. Chem. B. 113 (2009) 10521–10529.
[15] F. Chiti, P. Webster, N. Taddei, A. Clark, M. Stefani, G. Ramponi, C.M. Dobson, Designing conditions for in vitro formation of amyloid protofilaments and fibrils, Proc. Natl. Acad. Sci. U. S. A. 96 (1999) 3590–3594.
[16] N. Ostrov, E. Gazit, Genetic engineering of biomolecular scaffolds for the fabrication of organic and metallic nanowires, Angew. Chem. Int. Ed. Engl. 49 (2010) 3018–3021.
[17] E. van der Linden, P. Venema, Self-assembly and aggregation of proteins, Curr. Opin. Colloid Interface Sci. 12 (2007) 158–165.
[18] M.R. Nilsson, Techniques to study amyloid fibril formation in vitro, Methods 34 (2004) 151–160.

[19] P. Salomaa, L.L. Schaleger, F.A. Long, Solvent deuterium Isotope effects on acid-Base Equilibria, J. Am. Chem. Soc. 86 (1964) 1–7.
[20] F. Tanfani, T. Galeazzi, G. Curatola, E. Bertoli, G. Ferretti, Reduced beta-strand content in apoprotein B-100 in smaller and denser low-density lipoprotein subclasses as probed by Fourier-transform infrared spectroscopy, Biochem. J. 322 (Pt 3) (1997) 765–769.
[21] R. Eisert, L. Felau, L.R. Brown, Methods for enhancing the accuracy and reproducibility of Congo red and thioflavin T assays, Anal. Biochem. 353 (2006) 144–146.
[22] E.A. Ellis, Poststaining grids for transmission electron microscopy: conventional and alternative protocols, Methods Mol. Biol. 369 (2007) 97–106.
[23] S. Ahmad, M. Gromiha, H. Fawareh, A. Sarai, ASAView: database and tool for solvent accessibility representation in proteins, BMC Bioinform. 5 (2004) 51.
[24] O. Conchillo-Sole, N.S. de Groot, F.X. Aviles, J. Vendrell, X. Daura, S. Ventura, AGGRESCAN: a server for the prediction and evaluation of "hot spots" of aggregation in polypeptides, BMC Bioinform. 8 (2007) 65.
[25] E.F. Pettersen, T.D. Goddard, C.C. Huang, G.S. Couch, D.M. Greenblatt, E.C. Meng, T.E. Ferrin, UCSF, Chimera–a visualization system for exploratory research and analysis, J. Comput. Chem. 25 (2004) 1605–1612.
[26] J.C. Gordon, J.B. Myers, T. Folta, V. Shoja, L.S. Heath, A. Onufriev, H++: a server for estimating pKas and adding missing hydrogens to macromolecules, Nucleic Acids Res. 33 (2005) W368–W371.
[27] D.A. Case, T.A. Darden, T.E. Cheatham III, C.L. Simmerling, J. Wang, R.E. Duke, R. Luo, R.C. Walker, W. Zhang, K.M. Merz, B. Roberts, S. Hayik, A. Roitberg, G. Seabra, J. Swails, A.W. Goetz, I. Kolossvai, K.F. Wong, F. Paesani, J. Vanicek, R.M. Wolf, J. Liu, X. Wu, S.R. Brozell, T. Steinbrecher, H. Gohlke, Q. Cai, X. Ye, J. Wang, M.-J. Hsieh, G. Cui, D.R. Roe, D.H. Mathews, M.G. Seetin, R. Salomon-Ferrer, C. Sagui, V. Babin, T. Luchko, S. Gusarov, A. Kovalenko, P.A. Kollman, AMBER 11, University of California, San Francisco, 2011.ambermd.org.
[28] S.J. Weiner, P.A. Kollman, D.A. Case, U. Chandra Singh, C. Ghio, G. Alagona, S. Profeta, P. Weiner, A new force field for molecular mechanical simulation of nucleic acids and proteins, J. Am. Chem. Soc. 106 (1984) 765–784.
[29] B.J. Leimkuhler, R.D. Skeel, Symplectic numerical integrators in constrained Hamiltonian systems, J. Comp. Phys. 112 (1994) 117–125.
[30] M. Rueda, C. Ferrer-Costa, T. Meyer, A. Perez, J. Camps, A. Hospital, J.L. Gelpi, M. Orozco, A consensus view of protein dynamics, Proc. Natl. Acad. Sci. U. S. A. 104 (2007) 796–801.
[31] T. Darden, D. York, L. Pedersen, Particle Mesh Ewald - an N log(N) Method for Ewald Sums in large systems, J. Chem. Phys. 98 (1993) 10089–10092.
[32] S. Buzko, S.H. Pham, A. Taylor, Sirius v.1.2 (2009).http://www.ngbw.org/sirius/about.php.
[33] E.B. Getz, M. Xiao, T. Chakrabarty, R. Cooke, P.R. Selvin, A comparison between the sulfhydryl reductants tris(2-carboxyethyl)phosphine and dithiothreitol for use in protein biochemistry, Anal. Biochem. 273 (1999) 73–80.
[34] A. Ausili, B. Cobucci-Ponzano, B. Di Lauro, R. D'Avino, G. Perugino, E. Bertoli, A. Scire, M. Rossi, F. Tanfani, M. Moracci, A comparative infrared spectroscopic study of glycoside hydrolases from extremophilic archaea revealed different molecular mechanisms of adaptation to high temperatures, Proteins 67 (2007) 991–1001.
[35] M. Biancalana, S. Koide, Molecular mechanism of Thioflavin-T binding to amyloid fibrils, Biochim. Biophys. Acta. 1804 (2010) 1405–1412.
[36] M. Lindgren, P. Hammarstrom, Amyloid oligomers: spectroscopic characterization of amyloidogenic protein states, FEBS J. 277 (2010) 1380–1388.
[37] S. Kumar, S.K. Mohanty, J.B. Udgaonkar, Mechanism of formation of amyloid protofibrils of barstar from soluble oligomers: evidence for multiple steps and lateral association coupled to conformational conversion, J. Mol. Biol. 367 (2007) 1186–1204.
[38] A.R. Hurshman, J.T. White, E.T. Powers, J.W. Kelly, Transthyretin aggregation under partially denaturing conditions is a downhill polymerization, Biochemistry 43 (2004) 7365–7381.
[39] A.M. Morris, M.A. Watzky, R.G. Finke, Protein aggregation kinetics, mechanism, and curve-fitting: a review of the literature, Biochim. Biophys. Acta. 1794 (2009) 375–397.
[40] W. Colon, J.W. Kelly, Partial denaturation of transthyretin is sufficient for amyloid fibril formation in vitro, Biochemistry 31 (1992) 8654–8660.
[41] M. Fandrich, M. Schmidt, N. Grigorieff, Recent progress in understanding Alzheimer's beta-amyloid structures, Trends Biochem. Sci. 36 (2011) 338–345.
[42] J.L. Jimenez, E.J. Nettleton, M. Bouchard, C.V. Robinson, C.M. Dobson, H.R. Saibil, The protofilament structure of insulin amyloid fibrils, Proc. Natl. Acad. Sci. U. S. A. 99 (2002) 9196–9201.
[43] F.G. van der Goot, J.M. Gonzalez-Manas, J.H. Lakey, F. Pattus, A 'molten-globule' membrane-insertion intermediate of the pore-forming domain of colicin A, Nature 354 (1991) 408–410.